IEEE Access
Multidisciplinary ⋮ Rapid Review ⋮ Open Access Journal

Received 16 October 2023, accepted 10 January 2024, date of publication 15 January 2024, date of current version 2 February 2024.

Digital Object Identifier 10.1109/ACCESS.2024.3354707

RESEARCH ARTICLE

Research on Transformer Partial Discharge Fault Location Based on Improved UCA-RB-MUSIC Algorithm

YANLING LVY[1], KEXIAN AI[1], AND FENG GUO[2]
[1]School of Electrical and Electronic Engineering, Harbin University of Science and Technology, Harbin 150080, China
[2]Zhaoqing Power Supply Bureau of China Southern Power Grid, Zhaoqing 526000, China
Corresponding author: Yanling Lvy (yanling0828@163.com)

ABSTRACT Aiming at the problem that the coherent signal cannot be estimated when the traditional UCA-RB-MUSIC algorithm is used to detect the partial discharge of the transformer, an improved UCA-RB-MUSIC algorithm is suggested to reconstruct the signals captured by the array so that the number of calls sources is equivalent to the rank of the reconstructed signal matrix. The impact of correlated signals is eradicated. The results of simulation analysis and experimental verification show that when the improved UCA-RB-MUSIC algorithm is used to locate a single and double partial discharge source, the improved positioning error is only half of the mistake before improvement, which enhances the accuracy and resolution of uniform circular array positioning and the accuracy of transformer partial discharge detection.

INDEX TERMS Uniform circular array, partial discharge, power transformer, matrix reconstruction.

I. INTRODUCTION

Different techniques have been developed in the field of identifying and pinpointing partial discharge in transformers based on the observed phenomena associated with partial discharge both domestically and internationally. These techniques utilize various physical parameters that can effectively characterize the state of partial discharge in transformers, leading to a range of detection and localization methods. References [1], [2], [3], [4] employed the electrical localization technique to ascertain the precise electrical location of the partial discharge occurring within the transformer. However, because the pulse regularity of the partial discharge signals at different positions propagating to the end of the winding could be more robust, and the on-site electromagnetic interference is substantial, the electrical positioning method is challenging to apply in practice. In [5], the ultra-high frequency positioning method was employed to detect the electromagnetic signals of partial discharge in transformers. The positioning was based on analyzing the time delay relationship. However, due to the intricate internal structure of transformers, capturing the direct wave signals poses challenges. The sensor must be placed inside the transformer to receive the signal effectively, dramatically increasing the detection difficulty. Reference [6] employed the conventional ultrasonic positioning method to identify the location and timing of the ultrasonic waves generated by partial discharge, aiming to determine the source of the partial discharge. Due to the low sensitivity of a single acoustic sensor and the time delay estimation algorithm's accuracy limitations, the positioning results obtained through the traditional ultrasonic positioning method may suffer from significant errors, leading to inaccurate positioning. In [7], a technique for determining the position of a microphone array, which utilizes the MUSIC (Multiple Signal Classification) algorithm, is presented. The array composed of four sensors is used to receive partial discharge signals. This approach introduces a novel concept for localizing partisan discharge sources and overcomes the 'Rayleigh limit' constraint. However, when using a uniform circular array for positioning, the steering vector does not possess a Vandermonde structure, resulting in more complex calculations for subsequent steps. In [8], the pattern space transformation matrix is created to ensure that the steering vector of the uniform circular array exhibits a Vandermonde structure. The UCA-RB-MUSIC algorithm, as presented in [9], employs the MUSIC algorithm to estimate

The associate editor coordinating the review of this manuscript and approving it for publication was Yijie Wang.

the two-dimensional angle information of a signal by creating a beam transformation matrix with real-valued elements. This matrix construction approach enhances the accuracy of angle estimation and enables the localization of signal sources in a two-dimensional space.

This paper uses the research object of the dry-type transformer with 10 KV epoxy resin insulation. Aiming at the problem that the UCA-RB-MUSIC algorithm cannot shield the coherent signal, this paper proposes an improved UCA-RB-MUSIC algorithm for the transformer partial discharge fault location method. The rank of the reconstructed covariance matrix is adjusted to match the number of signal sources, enhancing the accuracy of angle estimation. This improves the identification and localization of signal sources in a two-dimensional space. Then, the orientation of each signal source can be obtained.

II. GENERATION MECHANISM AND CHARACTERISTICS OF TRANSFORMER PARTIAL DISCHARGE ACOUSTIC SIGNAL

When the epoxy resin is poured into the insulating dry-type transformer, if the process is not good, bubbles will be generated inside the epoxy resin, causing partial discharge. In epoxy resin, the presence of bubbles is a common occurrence. Due to the bubbles' lower dielectric coefficient than the insulating material, the electric field strength within the bubbles is significantly higher. As a result, the bubbles are more susceptible to breakdown and discharge. This paper mainly studies the air gap discharge caused by the existence of bubbles.

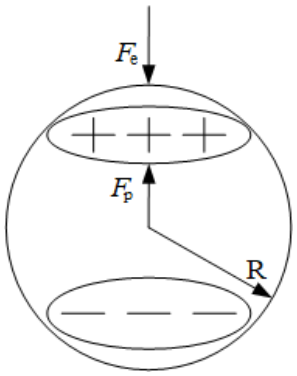

FIGURE 1. Bubble force diagram before discharge.

Suppose the bubble radius is R. Under typical conditions, the charge within the bubble is evenly distributed across both ends of the bubble due to the influence of the electric field. The bubble wall remains in equilibrium due to the combined effects of gas pressure F_p and electric field force F_e, as depicted in Fig. 1. When partial discharge occurs, the bubble is broken down quickly, suddenly causing the voltage at both ends to change to 0, and the bubble wall's mechanical equilibrium state is destroyed instantly. According to Newton's second law, the bubble wall expands rapidly outward under the action of gas pressure, and the bubble will also expand outward. As a result of the bubble wall's motion, it experiences additional forces, precisely the elastic force F_s, the friction force f, and the inertial force F_m of the bubble wall. These forces collectively generate the pressure that causes the bubble to expand outward, leading to the localized vibration of the bubble wall depicted in Fig. 2. The time for the bubble to be broken down is only nanoseconds. Therefore, the above process can be assumed to be a single pulse generated by partial discharge. The vibration process of the bubble wall occurs within microseconds, and this high-frequency vibration produces an ultrasonic signal.

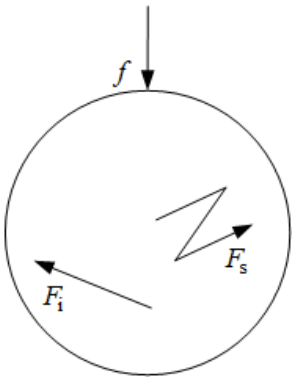

FIGURE 2. Bubble force diagram after discharge.

III. UNIFORM CIRCULAR ARRAY RECEIVING ACOUSTIC SIGNAL MODEL

Firstly, the model of a uniform circular array receiving acoustic signal is established, as shown in Fig. 3. The elements of an N-array are evenly distributed on a circular array with a constant radius of R, and each component of the array is independent, and not correlated with one another. Assuming that the acoustic signal is far enough, it can be considered a plane wave when it reaches the array. Additionally, the signal and noise are uncorrelated. Furthermore, it is assumed that the noise is a stationary, zero-mean Gaussian white noise with a variance of σ^2, and the noise received by each element of the microphone array is not correlated with the noise received by other components. Additionally, it is assumed that K (where K < N) independent and uncorrelated signal sources are arriving at the uniform circular array, and we establish a coordinate system with the center of the array (center of the circle) as the origin. The k-th signal source's azimuth and elevation angles relative to the uniform circular array are θ_k and φ_k, respectively.

Let $\boldsymbol{A} = \left[\boldsymbol{a}(\theta_1, \varphi_1)\, \boldsymbol{a}(\theta_2, \varphi_2) \cdots \boldsymbol{a}(\theta_K, \varphi_K)\right]$ be the uniform circular array's array manifold, and $\boldsymbol{a}(\theta_k, \varphi_k)$ be expressed as:

$$\boldsymbol{a}(\theta_k, \varphi_k) = \begin{bmatrix} \exp(\mathrm{j}\omega R \sin\theta_k \cos(\varphi_k - \gamma_0)/c) \\ \exp(\mathrm{j}\omega R \sin\theta_k \cos(\varphi_k - \gamma_1)/c) \\ \vdots \\ \exp(\mathrm{j}\omega R \sin\theta_k \cos(\varphi_k - \gamma_{N-1})/c) \end{bmatrix} \quad (1)$$

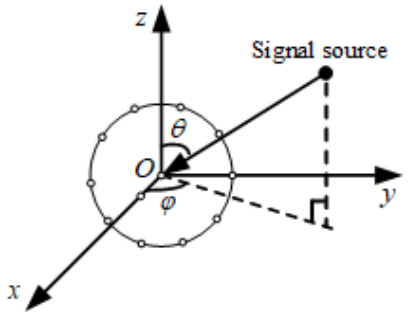

FIGURE 3. Uniform circular array.

where: $\gamma_n = 2\pi n/M, n = 0, 1, \cdots, N-1$, ω is the signal frequency, R is the radius of the circular array, and c is the speed of sound. And $\omega = 2\pi f, f/c = 1/\lambda$, a is the signal wavelength. Therefore, (1) can be rewritten as:

$$\boldsymbol{a}(\theta_k, \varphi_k) = \begin{bmatrix} \exp(\mathrm{j}2\pi R \sin\theta_k \cos(\varphi_k - \gamma_0)/\lambda) \\ \exp(\mathrm{j}2\pi R \sin\theta_k \cos(\varphi_k - \gamma_1)/\lambda) \\ \vdots \\ \exp(\mathrm{j}2\pi R \sin\theta_k \cos(\varphi_k - \gamma_{N-1})/\lambda) \end{bmatrix} \tag{2}$$

The received signal $\boldsymbol{x}(t) = [x_1(t), x_2(t), \ldots, x_N(t)]^{\mathrm{T}}$ of the uniform circular array can be expressed as:

$$\boldsymbol{x}(t) = \boldsymbol{A}\boldsymbol{s}(t) + \boldsymbol{n}(t) \tag{3}$$

Among them: $\boldsymbol{s}(t) = [s_1(t), s_2(t), \ldots, s_k(t)]^{\mathrm{T}}$ is the source vector, and $\boldsymbol{n}(t)$ is the noise received by the array. The complexity of the array manifold $\boldsymbol{A}$ in the uniform circular array results in a departure from the Vandermonde matrix structure, making it challenging to directly apply algorithms designed for uniform linear arrays that exhibit excellent performance.

IV. IMPROVEMENT OF THE UCA-RB-MUSIC ALGORITHM

A. UCA-RB-MUSIC ALGORITHM

For the signal model in (3), the covariance matrix $\boldsymbol{R}_x = \mathrm{E}[\boldsymbol{X}(t)\boldsymbol{X}^{\mathrm{H}}(t)]$ is a positive Hermitian square matrix, so it can be estimated by L signal snapshots using $\hat{\boldsymbol{R}}_x = (1/L)\sum_{l=1}^{L}[\boldsymbol{X}(t_l)\boldsymbol{X}^{\mathrm{H}}(t_l)]$. The feature decomposition of $\hat{\boldsymbol{R}}_x$ can be expressed as:

$$\hat{\boldsymbol{R}}_x = \boldsymbol{E}\boldsymbol{D}\boldsymbol{E}^{\mathrm{H}} = \boldsymbol{E}_s\boldsymbol{D}_s\boldsymbol{E}_s^{\mathrm{H}} + \boldsymbol{E}_n\boldsymbol{D}_n\boldsymbol{E}_n^{\mathrm{H}} \tag{4}$$

In (4), $\boldsymbol{D}$ represents a diagonal matrix formed by N eigenvalues of $\hat{\boldsymbol{R}}_x$, $\boldsymbol{D}_s$ is a diagonal matrix formed by K largest eigenvalues, and $\boldsymbol{D}_n$ is a diagonal matrix formed by the remaining $N-K$ smallest eigenvalues. $\boldsymbol{E}$ denotes a matrix composed of N eigenvectors of $\hat{\boldsymbol{R}}_x$, $\boldsymbol{E}_s$ consists of the eigenvectors corresponding to the K maximum eigenvalues, and $\boldsymbol{E}_n$ consists of the eigenvectors corresponding to the remaining $N-K$ small eigenvalues. $\boldsymbol{E}_s$ and $\boldsymbol{E}_n$ can be referred to as the signal subspace and noise subspace, respectively.

When the signal source is independent, there are some properties about the feature subspace: the subspace formed by the eigenvectors corresponding to the K largest eigenvalues is identical to the subspace formed by the direction vectors of the incoming signal, which can be represented as $\mathrm{span}\{\boldsymbol{e}_1, \boldsymbol{e}_2, \cdots, \boldsymbol{e}_K\} = \mathrm{span}\{\mathbf{a}(\Theta_1), \mathbf{a}(\Theta_2), \cdots, \mathbf{a}(\Theta_K)\}$. The signal subspace $\boldsymbol{E}_s$ is orthogonal to the noise subspace $\boldsymbol{E}_n$, meaning that $\mathbf{a}^{\mathrm{H}}(\Theta)\boldsymbol{e}_i = \boldsymbol{0}$, where $i = K+1, \cdots, N$.

To address the issue of the uniform circular array's array manifold $\boldsymbol{A}$ not having the Vandermonde matrix structure, the UCA-RB-MUSIC algorithm incorporates the mode space transformation matrix $\boldsymbol{F}_r^{\mathrm{H}}$. This transformation converts the uniform circular array into a virtual uniform linear array with a Vandermonde form array manifold. The mode space transformation matrix $\boldsymbol{F}_r^{\mathrm{H}}$ is unitary and is defined as:

$$\boldsymbol{F}_r^{\mathrm{H}} = \boldsymbol{W}^{\mathrm{H}}\boldsymbol{C}_v\boldsymbol{V}^{\mathrm{H}} \tag{5}$$

Of which:

$$\begin{cases} \boldsymbol{W} = \dfrac{1}{\sqrt{2M+1}}[\boldsymbol{v}(\alpha_{-M}), \cdots, \boldsymbol{v}(\alpha_0), \cdots, \boldsymbol{v}(\alpha_M)], \\ \alpha_i = \dfrac{2\pi i}{M}, i \in [-M, M] \end{cases} \tag{6}$$

Among them: $M = \lfloor (N-1)/2 \rfloor$ and $M > K, N$ represents the total number of elements in the uniform circular array, $\lfloor \bullet \rfloor$ is the downward integral function, so $N \geq 2M+1$.

And

$$\boldsymbol{v}(\alpha) = \left[e^{-jM\alpha}, \cdots, e^{-j\alpha}, e^{j0}, e^{j\alpha}, \cdots, e^{jM\alpha}\right]^{\mathrm{T}} \tag{7}$$

$$\boldsymbol{C}_V = \mathrm{diag}\left\{\mathrm{j}^{-M}, \cdots, \mathrm{j}^{-1}, \mathrm{j}^{0}, \mathrm{j}^{1}, \cdots, \mathrm{j}^{M}\right\} \tag{8}$$

$$\boldsymbol{V} = \sqrt{N}\,[\boldsymbol{w}_{-M}, \cdots, \boldsymbol{w}_0, \cdots, \boldsymbol{w}_M] \tag{9}$$

$$\boldsymbol{w}_m = \frac{1}{N}[1, e^{-\mathrm{j}2\pi m/N}, \cdots, e^{-\mathrm{j}2\pi m(N-1)/N}]^{\mathrm{T}} \tag{10}$$

According to the construction of $\boldsymbol{F}_r^{\mathrm{H}}$, $\boldsymbol{F}_r^{\mathrm{H}}$ is orthogonal, and $\boldsymbol{F}_r^{\mathrm{H}}$ is a $(2M+1) \times N$ -order matrix. The output data of the uniform circular array is transformed by $\boldsymbol{F}_r^{\mathrm{H}}$, as shown in (11), and the transformed receiving data matrix is $y(t)$, then

$$\boldsymbol{y}(t) = \boldsymbol{F}_r^{\mathrm{H}}\boldsymbol{x}(t) = \boldsymbol{F}_r^{\mathrm{H}}\boldsymbol{A}\boldsymbol{s}(t) + \boldsymbol{F}_r^{\mathrm{H}}\boldsymbol{n}(t) \tag{11}$$

According to (11), $\boldsymbol{F}_r^{\mathrm{H}}\boldsymbol{A}$ has the form of a Vandermonde array structure.

The covariance matrix of $\boldsymbol{y}(t)$ is

$$\boldsymbol{R}_y = \mathrm{E}[\boldsymbol{y}(t)\boldsymbol{y}^{\mathrm{H}}(t)] = \boldsymbol{F}_r^{\mathrm{H}}\boldsymbol{A}\boldsymbol{P}\boldsymbol{A}^{\mathrm{H}}\boldsymbol{F}_r + \sigma^2\boldsymbol{I} \tag{12}$$

Among them: $\boldsymbol{P} = \mathrm{E}[\boldsymbol{s}(t)\boldsymbol{s}^{\mathrm{H}}(t)]$, $\boldsymbol{I}$ is the unit matrix of order $(2M+1) \times (2M+1)$, and σ^2 is the noise power.

Eigenvalue decomposition is performed on $\boldsymbol{R}_y$. The signal subspace $\boldsymbol{S}$ consists of the feature vectors that correspond to the $\boldsymbol{K}$ largest eigenvalues, while the noise subspace $\boldsymbol{G}$ consists of the feature vectors that correspond to $(2M+1-K)$ smaller eigenvalues, that is,

$$\boldsymbol{S} = [\boldsymbol{s}_1, \boldsymbol{s}_2, \cdots, \boldsymbol{s}_P], \boldsymbol{G} = [\boldsymbol{g}_{P+1}, \boldsymbol{g}_{P+2}, \cdots, \boldsymbol{g}_{2M+1}] \tag{13}$$

The spatial spectrum function of the UCA-RB-MUSIC algorithm is formulated in the following manner:

$$f_{UCA-RB-MUSIC}(\theta,\varphi) = \frac{1}{(\boldsymbol{F}_r^{\mathrm{H}}\boldsymbol{a}(\theta,\varphi))^{\mathrm{H}}\boldsymbol{G}\boldsymbol{G}^{\mathrm{H}}(\boldsymbol{F}_r^{\mathrm{H}}\boldsymbol{a}(\theta,\varphi))} \tag{14}$$

The form of $\boldsymbol{a}(\theta,\varphi)$ in the equation is shown in (2). The direction angle estimates of the signal source can be obtained by identifying the azimuth and elevation angles corresponding to the K highest peaks of $f_{UCA-RB-MUSIC}(\theta,\varphi)$. In summary, the flow chart of the UCA-RB-MUSIC algorithm is shown in Fig. 4.

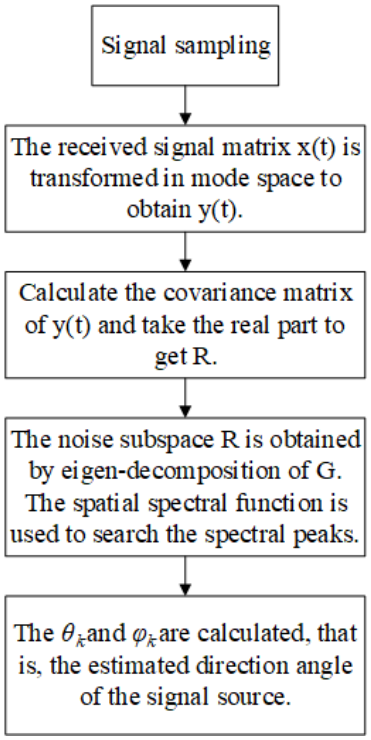

FIGURE 4. Flow chart of UCA-RB-MUSIC algorithm.

B. IMPROVED UCA-RB-MUSIC ALGORITHM

In the presence of coherent signal sources, coherent signals may be combined into one signal so that the number of independent sources arriving at the array will be reduced; that is, the rank of the source covariance matrix $\mathbf{R}_s$ is less than K. After performing the eigenvalue decomposition of the signal covariance matrix $\mathbf{R}_y$, if the number of obtained larger eigenvalues is more minor than K, then the corresponding signal subspace will also have fewer than K vectors. At this time, the direction vectors of some coherent signal sources will no longer be orthogonal to the noise subspace, so the direction angle estimation of the signal source will be incomplete; that is, the direction angle estimation of individual signals will be missing. To avoid this phenomenon and to ensure the estimation of azimuth for each signal source, the received signal's covariance matrix needs to be reconstructed, and the rank of the reconstructed matrix needs to be restored to K.

If let

$$\boldsymbol{y}(t) = \begin{bmatrix} \boldsymbol{y}_{-M}(t) \\ \vdots \\ \boldsymbol{y}_0(t) \\ \vdots \\ \boldsymbol{y}_M(t) \end{bmatrix}, \boldsymbol{F}_r^{\mathrm{H}} = \begin{bmatrix} \boldsymbol{F}_r^{\mathrm{H}}(-M) \\ \vdots \\ \boldsymbol{F}_r^{\mathrm{H}}(0) \\ \vdots \\ \boldsymbol{F}_r^{\mathrm{H}}(M) \end{bmatrix} \tag{15}$$

Then there is

$$\begin{cases} \boldsymbol{y}_k(t) = \boldsymbol{F}_r^{\mathrm{H}}(k)\boldsymbol{x}(t) = \boldsymbol{F}_r^{\mathrm{H}}(k)\boldsymbol{A}\boldsymbol{s}(t) + \boldsymbol{F}_r^{\mathrm{H}}(k)\boldsymbol{n}(t), \\ -M \le K \le M \end{cases} \tag{16}$$

Define the following correlation function:

$$\begin{aligned} r(k) &= \mathrm{E}[\boldsymbol{y}_0(t)\boldsymbol{y}_k^{\mathrm{H}}(t)] \\ &= \boldsymbol{F}_r^{\mathrm{H}}(0)\boldsymbol{A}\boldsymbol{P}\boldsymbol{A}^{\mathrm{H}}\boldsymbol{F}_r^{\mathrm{H}}(k) + \boldsymbol{\sigma}^2\delta_{0,k} \end{aligned} \tag{17}$$

where: when k is 0, $\delta_{0,k} = 1$; otherwise $\delta_{0,k} = 0$. When k changes from $-M$ to M in turn, the correlation function is $r(-M),\cdots,r(0),\cdots,r(M)$ in turn, and because of the orthogonality of $\boldsymbol{F}_r^{\mathrm{H}}$, it has:

$$r(k) = \begin{cases} \boldsymbol{F}_r^{\mathrm{H}}(0)\boldsymbol{A}\boldsymbol{P}\boldsymbol{A}^{\mathrm{H}}\boldsymbol{F}_r^{\mathrm{H}}(0) + \boldsymbol{\sigma}^2, k = 0 \\ \boldsymbol{F}_r^{\mathrm{H}}(0)\boldsymbol{A}\boldsymbol{P}\boldsymbol{A}^{\mathrm{H}}\boldsymbol{F}_r^{\mathrm{H}}(k), \quad k \ne 0 \end{cases} \tag{18}$$

The data vector $r(-M),\cdots,r(0),\ldots,r(M)$ contains the information of all signal sources, and the Toeplitz matrix is reconstructed from the data vector as follows:

$$\boldsymbol{R}_T = \begin{bmatrix} r(0) & r(1) & \cdots & r(M) \\ r(-1) & r(0) & \cdots & r(M-1) \\ \vdots & \vdots & \ddots & \vdots \\ r(-M) & r(-M+1) & \cdots & r(0) \end{bmatrix}_{(M+1)\times(M+1)} \tag{19}$$

Rank$(R_T) = M + 1$ can be known from the (19). To enhance the accuracy of the direction-finding algorithm, two-way smoothing of the $\boldsymbol{R}_T$ data is performed.

$$\tilde{\boldsymbol{R}}_T = \boldsymbol{R}_T + \boldsymbol{I}_v\boldsymbol{R}_T^*\boldsymbol{I}_v \tag{20}$$

where: $\boldsymbol{R}_T^*$ is the conjugate matrix of $\boldsymbol{R}_T$, $\boldsymbol{I}_v$ is defined as:

$$\boldsymbol{I}_v = \begin{bmatrix} 0 & 0 & \cdots & 1 \\ 0 & \cdots & 1 & 0 \\ \vdots & \vdots & \vdots & \vdots \\ 1 & 0 & \cdots & 0 \end{bmatrix}_{N\times N} \tag{21}$$

From (20), $\tilde{\boldsymbol{R}}_T$ is the unbiased estimate of $\boldsymbol{R}_T$ and rank$(\tilde{\boldsymbol{R}}_T) = M + 1 > K$. Feature decomposition of $\tilde{\boldsymbol{R}}_T$:

$$\tilde{\boldsymbol{R}}_T = \boldsymbol{U}_s\boldsymbol{D}_s\boldsymbol{U}_s^{\mathrm{H}} + \boldsymbol{U}_n\boldsymbol{D}_n\boldsymbol{U}_n^{\mathrm{H}} \tag{22}$$

where $\boldsymbol{U}_s$ represents the subspace of signals, and $\boldsymbol{U}_n$ denotes the subspace of noise. Likewise, the characteristic vector lies within the noise subspace.

Similarly, the feature vector in the noise subspace obtained by the $\tilde{\boldsymbol{R}}_T$ feature decomposition is substituted into the spatial spectrum function, and the calculation amount is much less than that of the UCA-RB-MUSIC method. At the same time, the direction estimation of the signal source will be more accurate, and the resolution effect of the algorithm will also be improved. The improved UCA-RB-MUSIC algorithm has better performance and better robustness.

C. THE STEPS AND FLOW CHART OF THE IMPROVED UCA-RB-MUSIC ALGORITHM

The proposed enhanced UCA-RB-MUSIC algorithm steps are as follows:

(1) Calculate the correlation function between each row of the received data matrix $\boldsymbol{y}(t)$ after the mode transformation and the received data of the $(M+1)$ row of $\boldsymbol{y}(t)$, and construct the Toeplitz matrix from the correlation function.

(2) The constructed Toeplitz matrix is bi-directionally smoothed.

(3) Signal subspace and noise subspace are obtained by feature decomposition.

(4) Spectrum peak searching based on noise subspace to estimate coherent sources' bearing estimation.

The flow chart of the improved UCA-RB-MUSIC algorithm is shown in Fig. 5.

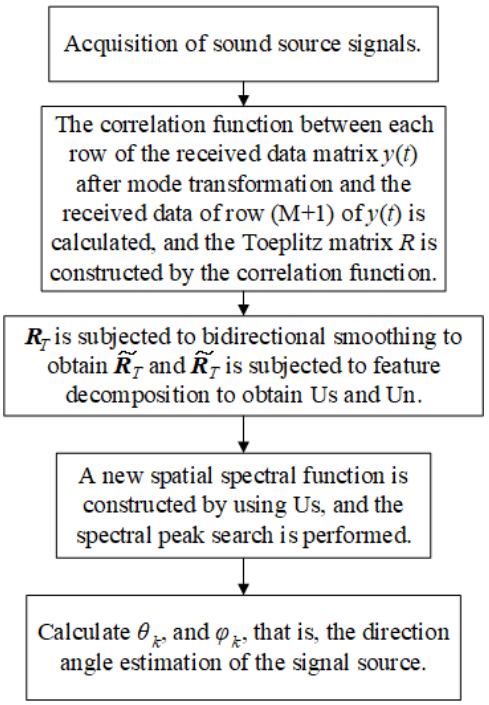

FIGURE 5. Flow chart of the improved UCA-RB-MUSIC algorithm.

V. TRANSFORMER PARTIAL DISCHARGE POSITIONING EXPERIMENTAL PLATFORM

The transformer partial discharge positioning experimental platform is divided into a partial discharge positioning system and a partial discharge signal simulation system. The former is mainly responsible for the partial discharge acoustic signal acquisition, analog-to-digital conversion, and digital partial discharge acoustic signal transmission, processing, and analysis; the latter generates a partial discharge acoustic wave simulation signal.

The structure diagram of the partial discharge positioning system is shown in Fig. 6.

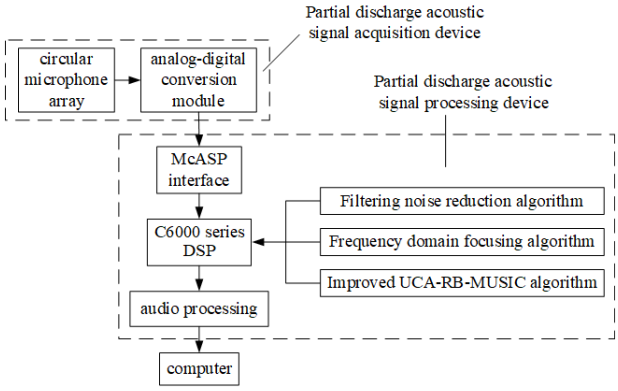

FIGURE 6. The structure diagram of the partial discharge location system.

The partial discharge localization system can be categorized into hardware and software components. Among them, the hardware part mainly includes the receiving and transmission system and signal processing hardware circuit; the software part mainly includes filtering noise reduction, frequency domain focusing, and acoustic positioning algorithm.

In the partial discharge positioning system designed in this paper, the selected processor is TMS320-C6748 DSP produced by TI company. Combined with the improved UCA-RB-MUSIC algorithm proposed above, the partial discharge source positioning test experiment is based on the eight-element microphone array. The physical connection diagram of the hardware part of the partial discharge positioning system is shown in Fig. 7. To judge the size of the array more intuitively, the Chinese one-yuan coin is used as a reference (the diameter of the one-yuan coin is 25 mm).

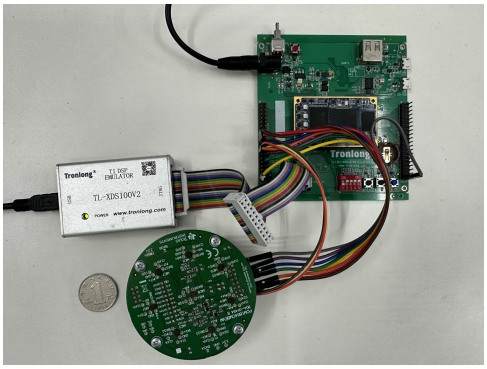

FIGURE 7. The structure diagram of the partial discharge location system.

The TMS320-C6748 processor is a multi-core processor chip. The circular microphone array TIDA-01454 has eight microphones. All eight microphones can collect acoustic signals with a flat frequency response and achieve 360-degree full-coverage acoustic acquisition. At the same time, the circular microphone array is also integrated with the ADC module PCM1864, which has a maximum sampling frequency of 384 kHz, and program statements can set the sampling frequency.

When the microphone collects the partial discharge acoustic signal, the ADC module PCM1864 integrated into the circular microphone array performs analog-to-digital conversion of the acoustic signal and saves the digitized acoustic signal. At the same time, PCM1864 is transmitted to DSP6748 utilizing a complex channel audio access interface (McASP interface) to facilitate the subsequent processing of digital acoustic signals. The McASP interface is a standard audio access interface for DSP produced by TI company in the United States, called the multi-channel audio access interface. In the partial discharge positioning system designed in this paper, McASP works in the receiving state and is connected to the ADC module PCM1864.

In this positioning system, DSP, as the primary device, addresses the slave station PCM1864 through the I2C bus and sends a control signal to the PCM1864 to control the clock acquisition mode, clock rate, and sampling rate of the PCM1864 audio decoder.

VI. SINGLE PARTIAL DISCHARGE SOURCE DIRECTION FINDING EXPERIMENT

To study the direction-finding performance of the improved UCA-RB-MUSIC algorithm, this section carries out the direction-finding experiment with the traditional UCA-RB-MUSIC algorithm. It compares the direction-finding results of the two. The acoustic signal of 70 - 180 kHz is selected to locate the partial discharge power supply to eliminate the influence of noise in the transformer itself and the surrounding environment.

By investigating the development process of different types of discharges and the waveform characteristics of current pulses, it is found that the partial discharge and the discharge process in air show similar development rules. The electronic pulse igniter can produce a stable broadband discharge signal whose discharge frequency range is identical to air gap discharge and has strong repeatability. Therefore, in this paper, an electronic pulse igniter with a working voltage of DC 1.5V and several discharge electrodes at the output end is selected as a partial discharge signal simulation system, and the discharge signal is employed to mimic the partial discharge signal produced by the transformer within the air gap.

Before the start of the experiment, there was no noise in the room except for the power supply to ensure that the experimental platform was empty and free of debris. The electronic pulse igniter is fixed to ensure that its axis passes through the center of the circular microphone array, and the axis's azimuth angle and pitch angle concerning the plane in which the circular microphone array is situated are recorded. In addition, the circular microphone array is ensured to be two meters away from the electronic pulse igniter.

A. SINGLE PARTIAL DISCHARGE SOURCE LOCALIZATION EXPERIMENT BASED ON UCA-RB-MUSIC ALGORITHM

In the first experiment, the electronic pulse igniter' s axis, which passes through the circular array's center, exhibits azimuth and pitch angles of −147° and 15°, correspondingly, relative to the plane where the microphone array is positioned. The RSS, in conjunction with the UCA-RB-MUSIC algorithm, is utilized to analyze and process the audio data captured by the circular microphone array, corresponding to partial discharge events. The direction-finding beam diagram is shown in Fig. 8.

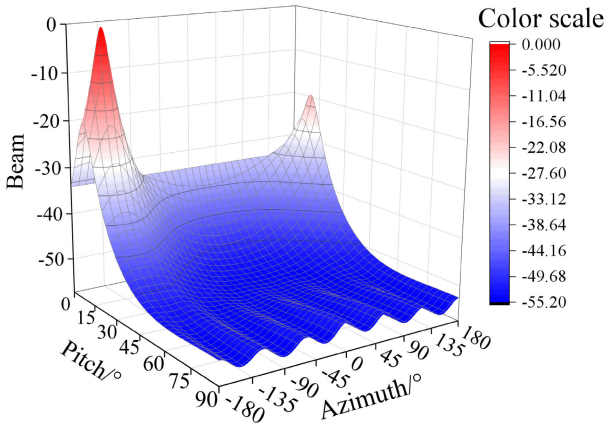

FIGURE 8. Using UCA-RB-MUSIC algorithm single partial discharge source direction finding beam pattern.

The angle formed by the axis of the electronic pulse igniter (passing through the center of the circular array) relative to the plane of the acoustic array sensor is changed many times. The direction-finding results of the UCA-RB-MUSIC algorithm are shown in Table 1 for five consecutive experiments on the same angle.

B. SINGLE PARTIAL DISCHARGE SOURCE LOCALIZATION EXPERIMENT BASED ON IMPROVED UCA-RB-MUSIC ALGORITHM

The audio data corresponding to partial discharge events, gathered by the circular microphone array in the previous article, are analyzed and processed using the RSS in conjunction with the enhanced UCA-RB-MUSIC algorithm. The beam pattern of the first group of direction-finding experiments is shown in Fig. 9.

The direction-finding results are shown in Table 2.

TABLE 1. The direction finding results of a single PD source.

Simulation group number	Actual angle		Simulation serial number	Direction finding angle of UCA-RB-MUSIC algorithm		Angular error average
	Azimuth	Pitch angle		Azimuth	Pitch angle	
1	-147	15	1	-153.6	11.1	7.559
			2	-156	11.6	
			3	-139.7	14.3	
			4	-142.6	14.3	
			5	-140.5	19.3	
2	-80	25	1	-76.3	30.3	6.215
			2	-85.7	21.1	
			3	-82.7	19.1	
			4	-84.4	22.8	
			5	-85.7	27.2	
3	-45	30	1	-49.9	26.2	6.849
			2	-49.8	27.4	
			3	-47.8	37	
			4	-37.1	31.3	
			5	-40.6	24.9	
4	70	60	1	71.9	70	8.174
			2	71.5	52	
			3	62.1	55.1	
			4	65.5	61.7	
			5	76.4	56.3	
5	-140	45	1	-136.8	43.2	6.331
			2	-134	50.3	
			3	-144.5	48.8	
			4	-138.4	51.7	
			5	-141	51.3	

TABLE 2. The direction finding results of a single PD source.

Simulation group number	Actual angle		Simulation serial number	Improved UCA-RB-MUSIC algorithm direction finding the angle		Angular error average
	Azimuth	Pitch angle		Azimuth	Pitch angle	
1	-147	15	1	-143	16.5	3.348
			2	-144.8	13.9	
			3	-145.3	11.8	
			4	-149.5	17.6	
			5	-149.1	13.9	
2	-80	25	1	-83.5	24.6	3.552
			2	-76	24.4	
			3	-76.8	23.8	
			4	-76.8	23.3	
			5	-82.8	26.3	
3	-45	30	1	-48	33.7	4.031
			2	-42.3	32.4	
			3	-47.9	27.4	
			4	-42.2	27.5	
			5	-41.3	31.6	
4	70	60	1	71	63.1	2.963
			2	72.8	57.9	
			3	68.9	62.8	
			4	71.5	61.1	
			5	68.2	62.3	
5	-140	45	1	-143.5	48	3.306
			2	-142.4	43.7	
			3	-137.2	46	
			4	-141.9	43.2	
			5	-138	47.5	

C. EXPERIMENTAL RESULT ANALYSIS

From Table 1 and Table 2, and according to the experimental error of the two algorithms, the error comparison is shown in Fig. 10.

Based on Fig. 10, it is evident that in each of the five sets of direction-finding experiments, the enhanced UCA-RB-MUSIC algorithm yields significantly lower errors than the UCA-RB-MUSIC algorithm for single PD source direction-finding. Furthermore, when comparing the results to Table 1 and Table 2, the maximum error of the enhanced UCA-RB-MUSIC algorithm is 4.031°, considerably smaller than the minimum error of the UCA-RB-MUSIC algorithm, which is 6.215°. Additionally, the calculations indicate that the average error of the former is only 3.44°, while the average

TABLE 3. The experimental results of dual partial discharge source direction finding based on the UCA-RB-MUSIC algorithm.

Simulation group number	Actual angle		Simulation serial number	Direction finding angle of UCA-RB-MUSIC algorithm		Angular error average
	Azimuth	Pitch angle		Azimuth	Pitch angle	
1	-140	45	1	-134	53.3	8.338
				-92.4	43.8	
			2	-134.9	49.9	
				-79.2	49.3	
	-83	45	3	-144.2	51	7.692
				-85.4	52	
2	13	30	1	21.3	30.9	7.359
				-158.6	32.7	
			2	19.9	30.1	
				-154.9	29.8	
	-164	30	3	17.7	34.8	7.516
				-170.9	31.6	
3	3	30	1	12.3	26	8.845
				-96.7	48.9	
			2	10.5	35.1	
				-113.8	58.3	
	-106	50	3	0	36.4	10.663
				-97.2	43.2	
4	43	30	1	48.4	37.9	9.455
				-87	49.2	
			2	33.7	25.9	
				-88.3	46	
	-79	45	3	51.3	32.1	9.353
				-74.8	53.7	
5	76	15	1	67.4	14.8	8.684
				-50.1	51.1	
			2	85.4	11.8	
				-55.3	68.5	
	-52	60	3	70.3	19.6	9.203
				-42.9	57.7	

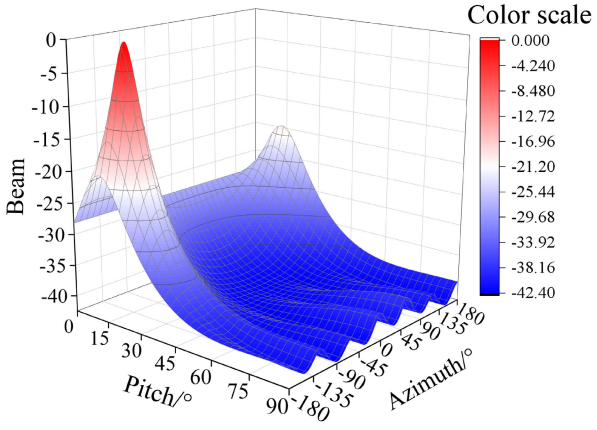

FIGURE 9. Using the improved UCA-RB-MUSIC algorithm single partial discharge source direction finding beam pattern.

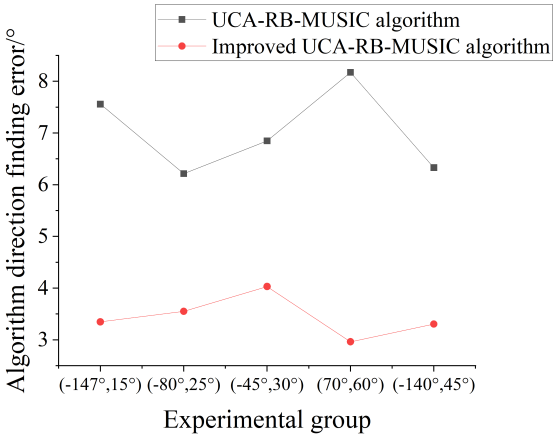

FIGURE 10. Using the improved UCA-RB-MUSIC algorithm single partial discharge source direction finding beam pattern.

error of the latter is 7.026°.In the single partial discharge source direction finding experiment, the error of the improved UCA-RB-MUSIC algorithm is only 50% of the traditional UCA-RB-MUSIC algorithm.

In summary, when it comes to the actual single partial discharge acoustic signal, the enhanced UCA-RB-MUSIC algorithm achieves a direction-finding accuracy of 4.5°, which surpasses that of the conventional UCA-RB-MUSIC algorithm. The improved UCA-RB-MUSIC algorithm demonstrates excellent direction-finding capabilities, making it well-suited for accurately determining the direction of a single partial discharge source in real-world environments.

VII. DOUBLE PARTIAL DISCHARGE SOURCE LOCALIZATION EXPERIMENT

In this experiment, electronic pulse igniters replicate the dual power supply for partial discharge simulation, with both igniters simultaneously emitting partial discharge signals. The other experimental conditions are the same as the single partial discharge source localization experiment.

A. DOUBLE PARTIAL DISCHARGE SOURCE LOCALIZATION EXPERIMENT

In the first experiment, the azimuth and pitch angles of the axis of the electronic pulse igniter (passing through the center of the circular array) relative to the plane of the microphone array were adjusted to −140° and 5°, respectively, while the elevation angles were set to −83° and 45°, correspondingly. The electronic pulse igniter was pressed to discharge continuously for 5 seconds during the experiment. At the same time, the circular microphone array began to collect the discharge signal at the moment of pressing. The waveform of the partial discharge signal during the first experiment is shown in Fig. 11. The RSS, in conjunction with the

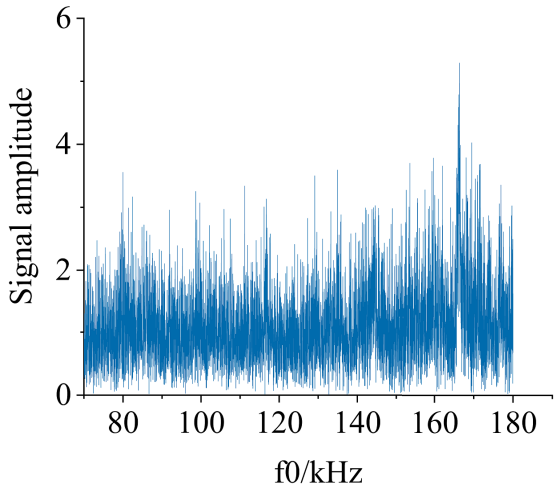

FIGURE 11. Double partial discharge source acoustic signal spectrum diagram.

UCA-RB-MUSIC algorithm, is utilized to analyze and process the audio data obtained from the circular microphone array, corresponding to the collection of partial discharge events. The beam pattern of the first direction-finding experiment is shown in Fig. 12.

The angle formed by the axis of the two electronic pulse igniters (both axes pass through the center of the circular microphone array) relative to the plane where the circular microphone array is located is changed multiple times. The direction-finding results based on the UCA-RB-MUSIC algorithm are shown in Table 3 for three consecutive experiments on the same set of angles.

B. DOUBLE PARTIAL DISCHARGE SOURCE LOCALIZATION EXPERIMENT BASED ON IMPROVED UCA-RB-MUSIC ALGORITHM

The positioning algorithm used in the experiment is changed to the improved UCA-RB-MUSIC algorithm. Other experimental conditions and parameters are unchanged, and the practical steps in Section VI are repeated. The RSS, in conjunction with the enhanced UCA-RB-MUSIC algorithm, is employed to analyze and process the audio data captured

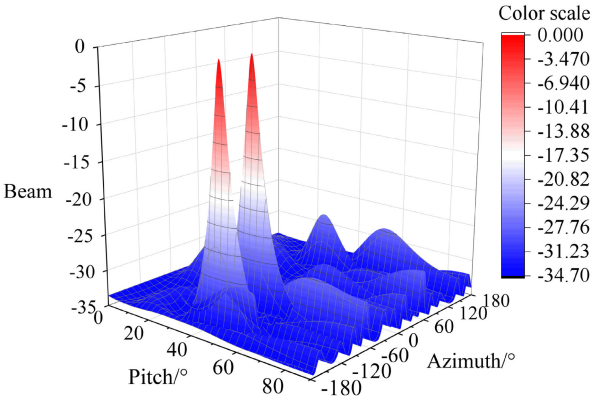

FIGURE 12. The experimental beam pattern of dual partial discharge source direction finding based on the UCA-RB-MUSIC algorithm.

by the circular microphone array, which corresponds to partial discharge events. The directional response of the initial direction-finding trial is illustrated in Fig. 13.

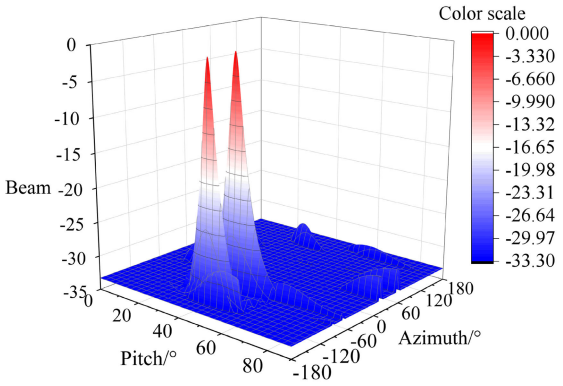

FIGURE 13. The experimental beam pattern of dual partial discharge source direction-finding based on improved UCA-RB-MUSIC algorithm.

Table 3 presents all the outcome data from the direction-finding experiments for the dual partial discharge source.

C. EXPERIMENTAL RESULT ANALYSIS

The data in Table 3 and Table 4 are compared, and the error pairs drawn according to the direction finding experimental error of the two algorithms are shown in Fig. 14. Among them, the unfilled data points indicate the errors generated by the UCA-RB-MUSIC algorithm. In contrast, the filled data points represent the errors the enhanced UCA-RB-MUSIC algorithm produces. The black angle coordinates below the horizontal axis represent the measured angles obtained from the first partial discharge source in the five sets of direction-finding experiments, and the red angle coordinate represents the measured angle of the five sets of direction-finding experiments of the second partial discharge source.

From Fig. 14, it is evident that the direction-finding error of the enhanced UCA-RB-MUSIC algorithm is considerably

TABLE 4. The experimental results of dual partial discharge source direction finding based on improved UCA-RB-MUSIC algorithm.

Simulation group number	Actual angle		Simulation serial number	Direction finding angle of UCA-RB-MUSIC algorithm		Angular error average
	Azimuth	Pitch angle		Azimuth	Pitch angle	
1	-140	45	1	-136.1	47.9	4.332
				-86.8	48	
			2	-143.2	47.2	
				-80.8	42.8	
	-83	45	3	-144.2	43.9	3.675
				-85.2	43.4	
2	13	30	1	18.2	29.2	4.969
				-160.1	28.4	
			2	17.2	32	
				-165.3	34.6	
	-164	30	3	10.5	34.3	4.576
				-168.5	28.6	
3	3	30	1	6.8	27.4	4.911
				-103	47.2	
			2	-0.3	26	
				-101.2	48.6	
	-106	50	3	7.3	32.4	4.559
				-102.7	53.1	
4	43	30	1	46.1	28.6	3.586
				-80.3	42.4	
			2	40.6	33.5	
				-77.6	41.6	
	-79	45	3	44.8	32.4	3.58
				-82.2	42.5	
5	76	15	1	72	16.1	4.068
				-49.4	61.4	
			2	78.5	18.1	
				-55.3	59.2	
	-52	60	3	74.3	18.7	3.488
				-50	63.5	

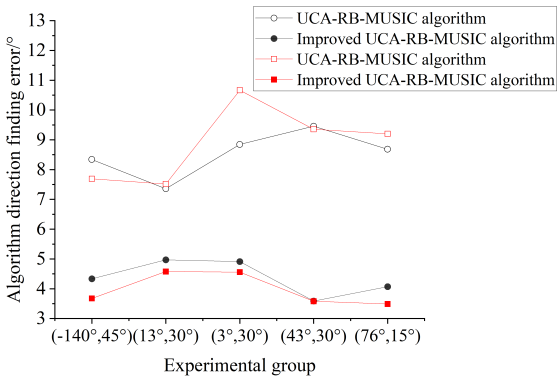

FIGURE 14. Two algorithms of double partial discharge source direction finding experiment error comparison diagram.

lower than that of the UCA-RB-MUSIC algorithm in all five sets of direction-finding experiments. At the same time, based on the information provided in Table 3 and Table 4, it can be observed that the enhanced UCA-RB-MUSIC algorithm exhibits a maximum error of 6.215°, which is significantly lower than the minimum error of the UCA-RB-MUSIC algorithm, which is 7.359°. Furthermore, the analysis indicates that the average error of the enhanced algorithm is 4.450°, while the average error of the conventional algorithm is 8.711°.In other words, in the direction finding experiment of double partial discharge sources, The enhanced UCA-RB-MUSIC algorithm exhibits an error rate of 51% of the error rate observed in the conventional UCA-RB-MUSIC algorithm.

According to the experimental findings, it has been demonstrated that the enhanced UCA-RB-MUSIC algorithm achieves a direction-finding accuracy of 5.0° for two absolute partial discharge acoustic signals. This accuracy surpasses that of the conventional UCA-RB-MUSIC algorithm. These results highlight the improved UCA-RB-MUSIC algorithm's excellent performance in direction-finding and its suitability for locating two partial discharge sources in real-world environments.

VIII. CONCLUSION

This paper introduces an enhanced UCA-RB-MUSIC algorithm to address the issue of unshielded coherent signal interference in detecting air gap discharge within epoxy resin-insulated dry-type transformers using the UCA-RB-MUSIC algorithm. The received signal covariance matrix is reconstructed to restore its rank to match the number of signal sources in the microphone array. Then, the positions of all partial discharge sources are obtained. The simulated and analyzed acoustic signal corresponds to a single partial discharge power supply and a dual partial discharge power supply. The results show that whether it is a single partial discharge power supply or a dual partial discharge power supply, the error of the results obtained by the improved UCA-RB-MUSIC algorithm is only 50% of the direction

finding results before the improvement. The direction-finding outcomes achieved by the enhanced UCA-RB-MUSIC algorithm exhibit a remarkable improvement compared to the results obtained before the enhancement. Then, the partial discharge experiment is carried out using the transformer partial discharge positioning experimental platform. The empirical findings align with the simulation results, which verify that the direction-finding error of the improved UCA-RB-MUSIC algorithm is only 50% of the direction-finding error before the improvement. It offers a benchmark approach for achieving more precise direction finding and localization of partial discharge in transformers.

REFERENCES

[1] J. Sun, S. Pan, and J. Deng, "Research status of partial discharge detection of power transformer based on pulse current method," *J. Phys., Conf. Ser.*, vol. 2195, no. 1, Feb. 2022, Art. no. 012024.

[2] D. Nascimento, S. S. Refaat, H. Loschi, Y. Iano, E. Chuma, W. El-Sayed, and A. Madi, "Current sensor optimization based on simulated transfer function under partial discharge pulses," *Sens. Actuators A, Phys.*, vol. 329, Oct. 2021, Art. no. 112825.

[3] J. Jiang, B. Zhang, Z. Li, P. Ranjan, J. Chen, and C. Zhang, "Partial discharge features for power electronic transformers under high-frequency pulse voltage," *IEEE Trans. Plasma Sci.*, vol. 49, no. 2, pp. 845–853, Feb. 2021.

[4] X. Zhang, G. Zhang, Y. Li, J. Zhang, and R. Huang, "On the feasibility of gap detection of power transformer partial discharge UHF signals: Gap propagation characteristics of electromagnetic waves," *Energies*, vol. 10, no. 10, p. 1531, Oct. 2017.

[5] K. C. Ghanakota, Y. R. Yadam, S. Ramanujan, V. J. V. Prasad, and K. Arunachalam, "Study of ultra high frequency measurement techniques for online monitoring of partial discharges in high voltage systems," *IEEE Sensors J.*, vol. 22, no. 12, pp. 11698–11709, Jun. 2022.

[6] L. Yongfen, J. Shengchang, and L. Yanming, "Phased-ultrasonic receiving-planar array transducer for partial discharge location in transformer," *IEEE Trans. Ultrason., Ferroelectr., Freq. Contr.*, vol. 53, no. 3, pp. 614–622, Mar. 2006.

[7] D. E. N. Davies, "A transformation between the phasing techniques required for linear and circular aerial arrays," *Proc. Inst. Electr. Eng. U.K.*, vol. 112, no. 11, p. 2041, 1965.

[8] Q. Guo and Y. F. An, "A unitary-UCA-root-MUSIC algorithm based on MSWF," *Appl. Mech. Mater.*, vol. 610, pp. 339–344, Aug. 2014.

[9] X. Pang, H. Wu, X. Li, Y. Qi, H. Jing, J. Zhang, and Q. Xie, "Partial discharge ultrasonic detection based on EULER-MUSIC algorithm and conformal array sensor," *IET Gener., Transmiss. Distrib.*, vol. 12, no. 14, pp. 3596–3605, Aug. 2018.

[10] C. P. Mathews and M. D. Zoltowski, "Eigenstructure techniques for 2-D angle estimation with uniform circular arrays," *IEEE Trans. Signal Process.*, vol. 42, no. 9, pp. 2395–2407, Sep. 1994.

YANLING LVY was born in Heilongjiang, China, in 1975. She received the Ph.D. degree in electrical engineering from the Harbin University of Science and Technology (HUST), Harbin, China, in 2010. She is currently a Professor with HUST. Her research interests include the operation and protection of large generators, generators and its system operation analysis, power system fault, and protection analysis.

KEXIAN AI was born in Henan, China, in 1999. He received the bachelor's degree in automation from the Henan Institute of Technology, Henan, in 2021. He is currently pursuing the master's degree with the School of Electrical and Electronic Engineering, Harbin University of Science and Technology, Heilongjiang. His main research interest includes transformer partial discharge detection.

FENG GUO was born in Jiangxi, China, in 1997. He received the bachelor's degree in electrical engineering and automation engineering from Nanchang University, Jiangxi, in 2015, and the master's degree in energy and power from the Harbin University of Science and Technology, Heilongjiang, China, in 2020. He is currently with Zhaoqing Power Supply Bureau of China Southern Power Grid. His main research interests include transformer fault diagnosis and partial discharge measurement.